Polyanion-mixed off-stoichiometric alluaudites Na3−δFe2±β(PO4)y(SO4)3−y as sustainable positive electrode materials for Na-Ion batteries

Anastasia Grebenshchikova, Jacob Olchowka, Loïc Simonin, Mathieu Duttine, François Fauth, Christian Masquelier, Laurence Croguennec

Polyanion-mixed Off-stoichiometric Alluaudites $Na_{3-\delta}Fe_{2\pm\beta}(PO_4)_y(SO_4)_{3-y}$ as Sustainable Positive Electrode Materials for Na-ion Batteries

Anastasia Grebenshchikova [1,2,3,5,6], Jacob Olchowka [1,5,6 *], Loïc Simonin [3], Mathieu Duttine [1], François Fauth [4], Christian Masquelier [2,5,6,7], Laurence Croguennec [1,5,6 *]

[1] Univ. Bordeaux, CNRS, Bordeaux INP, ICMCB, UMR 5026, F-33600 Pessac, France

[2] Laboratoire de Réactivité et de Chimie des Solides (LRCS), CNRS UMR 7314, Université de Picardie Jules Verne, Hub de l'Energie, Rue Baudelocque, 80039 Amiens Cedex, France

[3] Université Grenoble Alpes, CEA, LITEN, DEHT, LM 17 rue des Martyrs, Cedex 9, Grenoble, 38054, France

[4] CELLS-ALBA Synchrotron, Cerdanyola del Valles, 08290 Barcelona, Spain

[5] Réseau sur le Stockage Electrochimique de l'Energie (RS2E), CNRS FR 3459, Hub de l'Energie, Rue Baudelocque, 80039 Amiens Cedex, France

[6] ALISTORE-European Research Institute, CNRS FR 3104, Hub de l'Energie, Rue Baudelocque, 80039 Amiens Cedex, France

[7] Institut Universitaire de France, 103 boulevard Saint-Michel, F-75005 Paris, France

* Corresponding Authors: Laurence.croguennec@icmcb.cnrs.fr, Jacob.olchowka@icmcb.cnrs.fr

Keywords: Sodium-ion battery, positive electrode material, mixed polyanion compound, thermal treatment, alluaudite

Abstract

The transition to renewable energy sources requires cost-effective and scalable energy storage solutions, based on abundant elements, such as Na-ion batteries with sustainable positive electrode materials, based on Na, Fe and S. The sulfate-based alluaudite $Na_{2+2\delta}Fe_{2-\delta}(SO_4)_3$, that exhibits excellent cycling performance inspired the investigation of mixed PO_4^{3-}/SO_4^{2-} polyanion-based compounds with a view to increase the phase stability of sulfates. Herein, we report on various synthesis methods, such as solid-state, mechanochemical and ionothermal treatments to obtain -non reported until now compositions in the mixed phosphate-sulfate iron sodium alluaudite system, using the cost-effective precursors, Na_3PO_4 and $FeSO_4$. Quite surprisingly, solid-state synthesis followed *in situ* using synchrotron X-ray powder diffraction technique revealed the presence of an intermediate phase closely resembling the NaSICON phase $Na_{2.65}Fe_2PO_4(SO_4)_2$ along with $Na_6Fe(SO_4)_4$, prior to alluaudite formation. Physico-chemical investigations of the alluaudite $Na_{2.65}Fe_{1.9}(PO_4)_y(SO_4)_{3-y}$ (NFPS) phase, obtained via solid-state synthesis at 450°C, confirm that the phosphate incorporation enhanced the thermal stability while preserving promising electrochemical properties, *i.e.* rate capability and long-term stability with no capacity loss after 50 cycles: a reversible capacity of ≈90 mAh/g is obtained at an average discharge voltage of 3.32 V vs. Na^+/Na and for an electrode mass loading of 16 mg/cm^2. This study proposes easy and effective synthesis approaches to obtain series of compounds and opens the perspective to explore conditions of transitions between NaSICON and alluaudite structural types.

Introduction.

Na-ion batteries are now considered as a heavyweight alternative for more expensive Li-ion analogues, particularly for energy grid storage and low-range transport application. However, to ensure sustainability and low price of Na-ion battery supply chain, its components, especially positive electrode materials, should rely on abundant and inexpensive elements [1,2].The transition metal precursor often constitutes the most expensive reagent in the positive electrode material synthesis. While transition metals such as Co, Ni and V enable high-voltage redox reactions, their limited abundance drives the battery research community toward exploring new abundant and cheaper Fe-based compositions [3,4].

Among the various Fe-containing materials suitable for Na (de-)intercalation, such as layered oxides, Prussian blue analogues and polyanion compounds, the latter family stands out for its superior thermal and cycling stability, ensuring safety and longevity for the energy storage devices. The most widely studied Fe-based polyanion compounds as positive electrode materials in Na-ion batteries are built with phosphate or sulfate groups, and crystallize in the NaSICON or alluaudite structural types[5–8] .

The flexibility of the alluaudite structure, which enables 3D diffusivity of Na^+ ions, is a significant advantage in design and tuning the properties of positive electrode materials, making it highly attractive, as first shown by Trad *et al.* for phosphate alluaudite $NaMnFe_2(PO_4)_3$ [9] . More recently, Barpanda *et al*. [8] obtained a sulfate-based alluaudite, $Na_2Fe_2(SO_4)_3$ (NFS), by solid-state method with a remarkably high Fe^{3+}/Fe^{2+} operating voltage of 3.8 V (vs. Na^+/Na), induced by the sulfate groups, along with a quite interesting electrochemical performance (102 mAh/g at C/20).

Dealing with the synthesis of sulfate based alluaudites, the optimization and comprehension of aqueous synthesis routes have revealed that the formation of alluaudite phases results from the dehydration of intermediate hydrated sodium iron sulfate phases, such as kröhnkite and bloedite [10–13]. Recently, Yang *et al.* [14] also explored the relationships between intermediate phases that occur during spray drying synthesis by varying the $Na_2SO_4/FeSO_4{\cdot}7H_2O$ ratio. They identified the presence of bloedite, kröhnkite, and a "mesophase" $Na_xFe_y(SO_4)_z{\cdot}mH_2O$ ($x + 2y = 2z$, $0 \leq m < 4$), which is stable at 200 - 250°C.

Although aqueous methods are cost-effective and efficient, the resulting samples often exhibit poor electrochemical performance, prompting for the synthesis of alluaudites investigations into iono-and solvothermal approaches and revisiting solid-state [15]. The solid-state approach usually

ensures the purest alluaudite's samples, though understanding of the phase formation mechanism and off-stoichiometry origin is the key to optimization and control of the synthesis[16,17]. The main challenge in the alluaudite synthesis is presented by minimization of impurity quantities, which are usually residues of unreacted precursors ($FeSO_4$ and Na_2SO_4), preventing the iron oxidation leading to Fe_3O_4 and avoiding formation of the thermodynamically stable $Na_6Fe(SO_4)_4$ phase [11,18]. Additionally, Jungers *et al.*[13] have demonstrated that off-stoichiometric alluaudites $Na_{2+2\delta}Fe_{2-\delta}(SO_4)_3$ are more thermodynamically stable than the elusive stoichiometric $Na_2Fe_2(SO_4)_3$ due to the partial occupation of iron sites by sodium ions, which reduces Fe-Fe electrostatic repulsion within $Fe_{2-\delta}Na_{2\delta}O_{10}$ dimers. This phenomenon likely explains why a synthesis starting from stoichiometric ratios of $FeSO_4$ and Na_2SO_4 precursors often yields an alluaudite phase along with impurities and limited performance as a positive electrode material [13]. Indeed, in addition to its electrochemical inactivity, the common impurity $Na_6Fe(SO_4)_4$, characterized by a wide band gap (3.732 eV vs. 1.374 eV for NFS [14]), is believed to negatively impact the electrode performance by lowering its global electronic conductivity. However, it was also suggested that in some cases the heterostructure between $Na_6Fe(SO_4)_4$ and $Na_{2+2\delta}Fe_{2-\delta}(SO_4)_3$ (9 : 91 in weight ratio determined by XRD) could exhibit improved ionic kinetics due to 3D migration pathways of Na^+ ions in $Na_6Fe(SO_4)_4$, which acts as superionic conductor[19]. Increase of annealing temperature or extended thermal treatment to mitigate impurities formation remain usually not effective due to the decomposition of sulfate-based phases at relatively low temperatures[16,17]. A potential solution to this issue could be the design of polyanion-mixed compounds to increase alluaudite stability with the introduction of a polyanion group such as a phosphate $(PO_4)^{3-}$. To the best of our knowledge, only few studies have reported a synthesis approach of mixed phosphate-sulfate alluaudite phases [20, 21, 22]. In the first work, two alluaudites end members, $Na_2Fe_3(PO_4)_3$ and $Na_{2.56}Fe_{1.72}(SO_4)_3$, were synthesized and subsequently reacted in varying ratios to obtain several phases within the solid solution $Na_xFe_y(PO_4)_{3-z}(SO_4)_z$ (z = 0, 1, 1.5, 2, 3). Although elegant, this sophisticated synthetic procedure requires the use of 7 precursors and involves 6 distinct reactions, posing significant limitations for scalability. More recently, a simpler approach to obtain $Na_{2.9}Fe_{1.7}(SO_4)_{2.7}(PO_4)_{0.3}$ was reported[20] . This process used ball milling of $FeSO_4$, Na_3PO_4 and Na_2SO_4, followed by annealing, to produce the mixed polyanion compound. Besides, the authors have reported that the resulting $Na_{2.9}Fe_{1.7}(SO_4)_{2.7}(PO_4)_{0.3}$ alluaudite still maintains its original crystal structural and sodium-storage property after one-week exposure to air, unlike pure sulfate-based compounds. The same group reported the preparation of a novel Fe-fully occupied phase-pure

$Na_{2.5}Fe_2(SO_4)_{2.5}(PO_4)_{0.5}$ with promising performance such as high capacity retention over 88% after 10 000 cycles at 10C. Similar motivations drove us to further study and understand the synthesis reaction mechanism of such mixed polyanion phases, with the expectation to better control their composition, and thus to increase their theoretical capacity. Note that Liu *et al.*[20] proposed an increased air stability for these mixed polyanionic materials, an added-value for the battery manufacturing step.

Here, we report on three new different synthesis routes for sodium iron phosphate-sulfate (NFPS) alluaudite phases. Starting with a mixture of the inexpensive and available precursors Na_3PO_4 and $FeSO_4$ in molar ratio 1 : 2, we investigated ionothermal, mechanochemical and solid-state synthesis conditions, to obtain NFPS alluaudite phases. As one of the goals was also to follow the phase formation, particular emphasis was placed on the solid-state synthesis approach, with variation of annealing time and temperature under an inert atmosphere. Besides, we monitored in real time the synthesis by *in situ* synchrotron X-ray thermo-diffraction to study the reaction mechanism and identify the optimal reaction temperature range. Interestingly, this experiment reveals that a NaSICON intermediate phase was formed during heating, suggesting better thermodynamic stability of alluaudite versus NaSICON in Fe^{2+}-based sodium phosphate-sulfate compounds. Finally, the energy storage performance of the $Na_{2.65}Fe_{1.9}(PO_4)_y(SO_4)_{3-y}$ compound, tested in Na-metal half-cell showed significant promises.

Experimental methods

***Synthesis*.**

Dehydrated sodium phosphate (Na_3PO_4) and almost anhydrous home-prepared $FeSO_4{\cdot}xH_2O$ ($x \approx 0.08$) were used for the synthesis of mixed phosphate-sulfate alluaudites via three different synthesis routes: solid-state, ionothermal and mechanochemical. The Na_3PO_4 precursor was obtained by heating $Na_3PO_4{\cdot}10H_2O$ (Sigma-Aldrich, 95%) for 3h at 200°C under vacuum, whereas $FeSO_4{\cdot}xH_2O$ ($x \approx 0.08$) was prepared through the dehydration of iron sulfate $FeSO_4{\cdot}7H_2O$ (ReagentPlus®, ≥ 99%) by annealing under an argon flow for 3h at 250°C. The chemical composition and residual content in H_2O of both precursors were checked by chemical (ICP-OES, for inductively coupled plasma - optical emission spectrometry) and thermogravimetric (TGA) analyses. Besides, Mössbauer spectroscopy measurements confirmed that iron (II) was not

oxidized during this dehydration process. Once dehydrated, all the following manipulations with precursors and obtained samples were performed in an Ar-filled glove box.

First, the powders of $FeSO_4$ and Na_3PO_4 (in a molar ratio 2 : 1) were weighted, mixed in a mortar and put into a ZrO_2 ball milling jar to be subjected to thorough mixing via ball milling in SPEX SamplePrep 8000 mixer/mill for 1 hour with ball-to-powder mass ratio of 20 : 1. The resulting mixture was then used for the solid-state and ionothermal reactions. It is important to mention that no reactivity between $FeSO_4$ and Na_3PO_4 was observed during this process, as it will further be observed during *in situ* experiments.

Solid-state reaction: the ball milled powder was pressed into 8-mm diameter pellets and annealed at 450°C during 15 h in sealed gold tubes under Ar atmosphere. Different synthesis conditions of annealing, such as longer duration (25 h) and higher temperatures (480°C and 510°C) were tested as further described.

Ionothermal: 500 mg of powder after ball milling was transferred into a 45 ml Teflon Parr reactor to which 5 ml of ionic liquid 1-Ethyl-3-methylimidazolium bis(trifluoromethylsulfonyl) imide (EMIM-TFSI; IoLiTec, ≥97%) (dehydrated with hot molecular sieves) was added. Once sealed in the glovebox, the stainless-steel autoclave was heated for 24 h at 250°C with an isothermal heating collar from IKA under a constant stirring. Then, the powder was recovered by centrifugation with absolute ethanol and dried at 80°C under vacuum.

Mechanochemical synthesis: this third synthesis approach consisted of mixing the precursors in a mortar, followed by ball milling in hermetically sealed under argon ZrO_2 jars using a Planetary Micro Mill PULVERISETTE 7 premium line (Fritsch). Balls-to-powder mass ratio was equal to 10 : 1 and the total duration of synthesis was estimated as 12.5 hfor 50 cycles, each cycle being 15 min long, consisting of 10 min of milling and 5 min of rest for heat dissipation.

Characterization of the pristine new material.

X-ray powder diffraction patterns were collected with a Bruker D8 Discover diffractometer in Debye-Scherrer mode in the 2-30° 2θ range with a step size of 0.02°, using a MoKα radiation. Capillaries (diameter of 0.5 mm) were filled and sealed in an Ar-filled glove box in order to prevent any evolution of the material by contact with ambient air during the XRD pattern acquisition. The data analysis was performed using the GSASII computing software [23]. The

background was fitted with a Chebyshev polynomial function, and the peak profile with a pseudo-Voigt function.

The elemental composition of Na, Fe, P and S in the samples and precursors was determined by ICP-OES using a Varian ICP-OES 720 ES spectrometer. To prepare the solutions, the powders were dissolved in a mixture of 5 ml of concentrated HCl and HNO_3 in volume ratio 1 : 2, then the obtained solutions were diluted by deionized water. Calibration solutions were prepared by mixing standard solutions for Na, Fe, P and S, and the wavelengths of 589.592 nm, 234.350 nm, 178.222 nm and 180.699 nm, respectively, were used.

The morphology of the particles was analyzed with a scanning electron microscope (SEM) TESCAN VEGA with prior gold deposition.

^{57}Fe Mössbauer spectroscopy experiments were carried out at T = 298K with a constant acceleration Halder-type spectrometer in transmission geometry with ^{57}Co source (embedded in Rh matrix). The calibration of the velocity scale was performed with the characteristic sextet of a pure α-Fe^0 foil as reference. Refinement of the Mössbauer hyperfine parameters was performed with WinNormos software (Wissenschaftliche Elektronik GmbH).

Synthesis followed *in situ* by *Synchrotron X-ray powder diffraction* (SXRPD).

In situ temperature-controlled X-ray diffraction measurements were performed at the MSPD beamline of the ALBA-Cells synchrotron in Cerdanyola del Vallès, Spain [24]. The initial ball milled mixture of precursors ($FeSO_4$ and Na_3PO_4 in molar ratio 2 : 1), verified by ICP-OES, was heated in a 0.7 mm diameter quartz capillary with a hot air blower (FMB Oxford) positioned above the capillary. The temperature calibration was done with a second thermocouple at the blower's tip, while thermal expansion of Si powder was used as reference. 220 patterns in the 2θ angular range of 2 - 60°, with a 2θ step size of 0.006°, were collected by the position sensitive detector MYTHEN-II with the wavelength of 0.8269 Å every 63 seconds.

***Electrode preparation and electrochemical experiments*.**

$Na_{2.65}Fe_{1.9}(PO_4)_y(SO_4)_{3-y}$, obtained by solid-state method, was mixed in a mortar in an Ar-filled glove box with Ketjen Black (EC-600JD, Lion Specialty Chem.) in mass ratio 80 : 20 and transferred to 10 ml agate jar before being ball milled in SPEX SamplePrep 8000 mixer/mill for 40 min. All

further manipulations were performed in the glove box. After milling the mixture was collected from the jar and mixed in a mortar with polytetrafluoroethylene (PTFE, Sigma Aldrich) in weight ratio 95 : 5 to prepare free-standing electrodes in order to avoid reaction with air or moisture. Disks of 8 mm in diameter and, approximately of 0.25 mm in thickness, were cut and served as positive electrodes in CR2032-type coin-cells with Na metal as a reference and negative electrode. The active mass loading of the resulting positive electrodes, obtained by this dry method, ranged between 16 and 25 mg/cm². One sheet of Viledon filter between 2 sheets of Celgard separators were used, the electrolyte composition was 1 M $NaPF_6$ (Strem Chemicals; ≥99%) in a 1 : 1 (mass ratio) mixture of ethylene carbonate and dimethyl carbonate with 2 wt% of fluoroethylene carbonate. All cells were tested in a voltage range of 2.2 V - 4.5 V vs. Na^+/Na and at different cycling rates. Capacity retention upon cycling at different discharge D-rates from D/30 to 2D was tested for Na-half cells with charge C-rates kept at C/30.

Results and discussions

Insights in the synthesis of alluaudite-type sodium iron mixed phosphate-sulfate phases

***Synthesis methods exploration and phase identification*.** The primary objective of this work was to investigate various possibilities to obtain sodium iron mixed phosphate-sulfate phases (NFPS), starting from cheap and abundant dehydrated $FeSO_4$ and Na_3PO_4 precursors.

The solid-state method was chosen as a conventional synthesis approach to demonstrate the direct formation of NFPS from selected precursors. Although our protocol utilizes only two precursors, pre-mixing by ball milling was employed to ensure homogeneity of the reactant mixture and therefore, better diffusion during the annealing process. Since the reaction between these precursors is not expected to evolve gas, we also considered solely mechanochemical synthesis as a strategy to stabilize the targeted compound. Finally, the feasibility of formation of a mixed phosphate-sulfate phase in a liquid medium at moderate temperatures was also explored using ionothermal reaction. The complexity of this system includes preferential stabilization of off-stoichiometric alluaudites in terms of Na and Fe contents with existence of full range of solid solutions between phosphates and sulfates. On the other hand, thermodynamic and kinetic limitations of the chosen synthesis method also influence the product's composition.

Indeed, annealing and ionothermal techniques usually favor formation of more thermodynamically stable phases, while ball milling allows to obtain metastable phases.

The XRD patterns of the samples synthesized via ionothermal, solid-state and mechanochemical methods, are shown in **Figure 1**. All three XRD patterns contain a dominant alluaudite phase, indexed in the *C*2/*c S.G.*, with diffraction peak positions close to the ones reported for $Na_{2.37}Fe_{2.15}PO_4(SO_4)_2$ [21]. Cell parameters and refined Na/Fe ratio of the alluaudite phases are reported in **Table 1**, with details of the Rietveld refinements provided later hereafter in the text and in corresponding Supplementary Information. The difference in the cell parameters coupled with various Na/Fe ratios could arise from deviations in anion stoichiometry, affected by the presence of different impurities, as the nature and molar ratios of the reactants remained unchanged. Indeed, the sample after ionothermal treatment contains only 76.4(5) wt% of mixed polyanion alluaudite phase and displays a large amount of impurities: 18.7(1) wt% of $Na_6Fe(SO_4)_4$ and 4.9(2) wt% of $Fe_{3.08}(PO_4)_{2.04}O_{0.51}(OH)_{1.33}$. The latter could be formed due to residues of water left in the ionic liquid, as the precursors themselves were dried before the synthesis. Due to difficulty of XRD to distinguish between P and S atoms, the stoichiometry of the alluaudite phase was fixed to 1 : 2 for the refinements. However, the actual P/S ratio can deviate from the targeted 1 : 2, as suggested by the presence of impurities, which motivates us to attribute the chemical compositions of the series of compounds as $Na_{3-\delta}Fe_{2\pm\beta}(PO_4)_\gamma(SO_4)_{3-\gamma}$. On the other hand, the Na/Fe ratio in the alluaudite phases could be refined based on obtained XRD data. Ionothermal synthesis produced a sample with Na/Fe ratio of 3 : 1.9, which could be considered as a Na-rich alluaudite phase, especially compared to the one reported by Yamada's group [21], *i.e.* 2.37 : 2.15. Albeit the presence of impurity (24 wt%) and thus requiring optimization of synthesis conditions, to the best of our knowledge this mixed phosphate-sulfate alluaudite phase was the first obtained by ionothermal method.

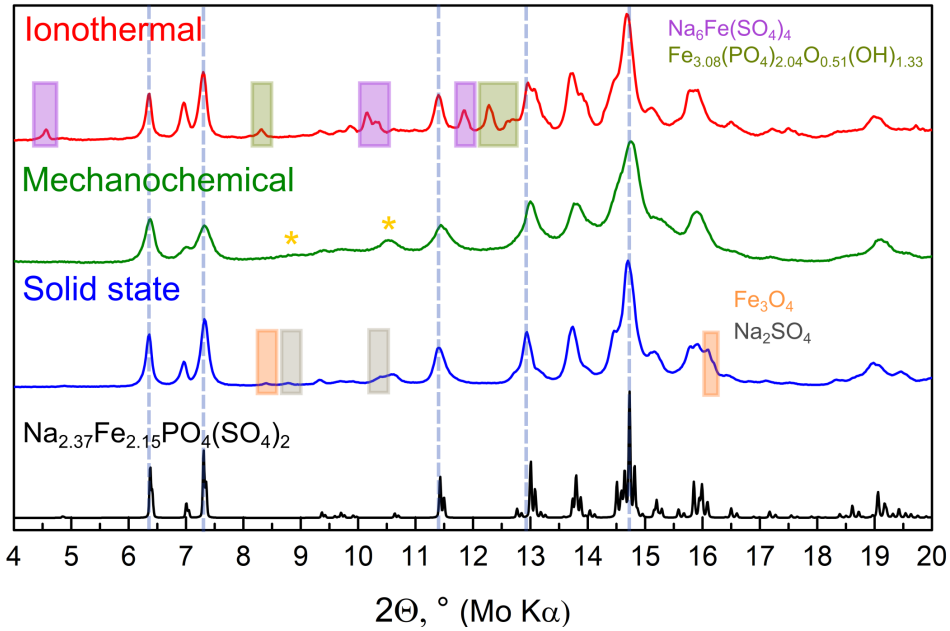

Figure 1. XRD patterns of three samples synthesized via different methods: ionothermal, mechanochemical and solid-state. For reference, the XRD pattern of $Na_{2.37}Fe_{2.15}PO_4(SO_4)_2$ is provided (PDF #04-024-6271). Typical impurities found in sulfate alluaudites are highlighted with colored rectangles: violet for $Na_6Fe(SO_4)_4$ (COD #7130195); pistachio for $Fe_{3.08}(PO_4)_{2.04}O_{0.51}(OH)_{1.33}$ (ICSD #91193); orange for Fe_3O_4 (ICSD #26410) and grey for Na_2SO_4 (ICSD #81505). Yellow asterisks highlight unindexed peaks, and thus attributed to any impurity.

Mechanochemical synthesis allowed to obtain a sample with lower crystallinity, as seen from the broader diffraction peaks of its XRD pattern, compared to the two other patterns (**Figure 1**): its coherent domain size is ≈30 nm (**Table 1**) vs. more than 150 nm for those obtained by solid-state and ionothermal reactions. Interestingly, two non-indexed peaks in the *C*2/*c S.G.* at 8.82°2θ and at 10.65°2θ could be attributed to an unidentified impurity and a microstructural effect, respectively. The alluaudite's phase composition determined by Rietveld refinement is $Na_{2.26}Fe_{2.42}(PO_4)_y(SO_4)_{3-y}$ and represents the first successful synthesis of a sulfate-containing sodium iron alluaudite solely through mechanochemical treatment without additional annealing. Finally, annealing of the $FeSO_4/Na_3PO_4$ mixture (2 : 1 molar ratio) at 450°C during 15h provided an alluaudite phase of $Na_{2.65}Fe_{1.9}(PO_4)_y(SO_4)_{3-y}$ composition (with 88.4(5) wt% of alluaudite in the sample, 9.7(1) wt% of Na_2SO_4 and 1.9(6) wt% of Fe_3O_4). Compared to the ionothermal route, the solid-state thermal treatment ensures a larger fraction of the alluaudite phase in the sample.

Table 1. Cell parameters and coherent domain sizes obtained from Rietveld refinement for the 3 samples synthesized by different methods (ionothermal, mechanochemical and solid-state) and compared to reference literature data of $Na_{2.37}Fe_{2.15}PO_4(SO_4)_2$ (PDF #04-024-6271).

Sample	Cell parameters of $Na_{3-\delta}Fe_{2\pm\beta}(PO_4)_y(SO_4)_{3-y}$, *C2/c S.G.*, *Z* = 4					GOF R_{wp}	Coherent domain size, nm
	***a*, Å**	***b*, Å**	***c*, Å**	***β*, °**	***V*, Å³**		
Ionothermal $Na_3Fe_{1.93}(PO_4)_y(SO_4)_{3-y}$	12.33(1)	12.785(1)	6.588(4)	115.44(2)	937.6(1)	2.14 3.28	160
Mechanochemical $Na_{2.26}Fe_{2.42}(PO_4)_y(SO_4)_{3-y}$	12.21(2)	12.724(3)	6.552(5)	115.20(2)	921.4(5)	2.09 2.61	33
Solid-state $Na_{2.65}Fe_{1.9}(PO_4)_y(SO_4)_{3-y}$	12.299(1)	12.803(1)	6.605(4)	115.468(1)	939.01(1)	3.27 3.73	190
$Na_{2.37}Fe_{2.15}PO_4(SO_4)_2$ **by Lu *et al*** [21]**.**	12.317	12.756	6.563	115.35	931.86	-	

We hence revealed that sodium iron phosphate-sulfate alluaudite phases could be obtained from Na_3PO_4 and $FeSO_4$ precursors not only by classic solid-state method, but also by mechanochemical and ionothermal reactions, though the reported synthesis conditions for the latter require further optimization. This section also highlighted the versatility of the alluaudite composition, depending on the synthesis method and underscores the necessity to employ various synthesis approaches to obtain new compositions. Considering the easier up-scale possibility of solid-state synthesis, compared to the two others, further exploration and optimization were conducted on solid-state synthesis method in the following part.

In order to explore the impact of temperature and annealing duration on alluaudite sample composition, syntheses were carried out at temperatures of 450°C, 480°C and 510°C with the same annealing time of 15h. In parallel, the annealing time was increased to 25h for the synthesis conducted at 450°C, as reported in **Table 2**. The associated XRD patterns and samples compositions obtained after Rietveld refinements are shown in **Figure 2**.

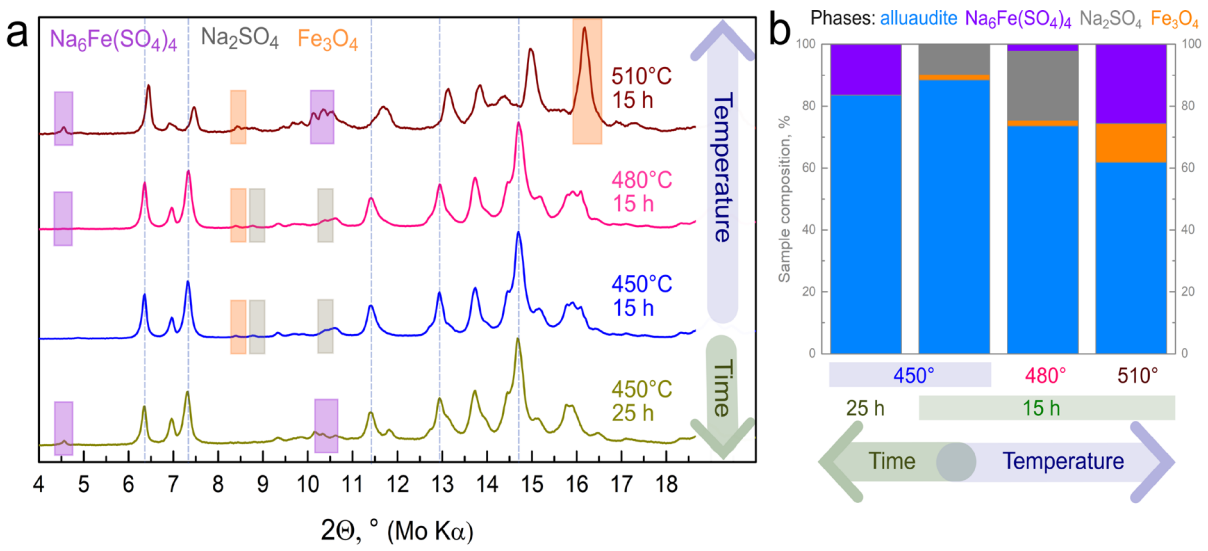

Figure 2. (a) XRD patterns of the samples obtained by solid-state synthesis at different temperatures and with increased duration of the annealing; **(b)** weight fractions of the various phases in these samples (blue for the alluaudite phase, violet for $Na_6Fe(SO_4)_4$, grey for Na_2SO_4 and orange for Fe_3O_4).

The largest fraction of alluaudite $Na_{2.65}Fe_{1.9}(PO_4)_y(SO_4)_{3-y}$ (88.4(5) wt%) was obtained from the synthesis carried out at 450°C. Thermal treatment of the precursors' mixture at 480°C resulted in a decrease in alluaudite fraction to 74(2) wt% and an increase in the Na_2SO_4 fraction up to 22(2) wt%, likely due to the decomposition of alluaudite. This result supports the previous study demonstrating the existence of a possible solid solution $Na_xFe_y(PO_4)_z(SO_4)_{3-z}$ ($0 \leq z \leq 3$) [21]. An increase of the synthesis temperature further to 510°C reduces the alluaudite phase fraction to 62(1) wt%, while increasing the $Na_6Fe(SO_4)_4$ fraction to 26(1) wt%. In general, in the temperature range of 450 - 510°C the amount of impurities is directly linked to the sample's composition: the higher is the synthesis temperature, the largest amount of impurities and the lower the Na/Fe ratio in the alluaudite phase is observed (see **Table 2**).

Prolonged annealing for 25 h at 450°C (compared to 15 h) slightly reduces the alluaudite fraction from 88.4(5) wt% to 83.5(3) wt% and almost does not change its sodium-to-iron ratio about 1.4 in $Na_{2.82}Fe_{2.02}(PO_4)_y(SO_4)_{3-y}$, with the formation of $Na_6Fe(SO_4)_4$ instead of Na_2SO_4 and Fe_3O_4, as mentioned in **Table 2.** Therefore, these experiments demonstrate that temperature is a more important factor in the solid-state synthesis of the mentioned mixed phases, rather than time, as increase of the temperature from 450°C to 510°C favors decrease of alluaudite's fractions. Note also that at 510°C y is probably close to 3 with the formation of an almost phosphate-pure alluaudite with iron at the divalent state mainly.

Table 2. Refined phase composition of the samples, obtained by solid-state synthesis with variation of temperature and annealing time.

Synthesis conditions		Phase mass fractions				
t, h	T, °C	Alluaudite		Fe_3O_4	Na_2SO_4	$Na_6Fe(SO_4)_4$
		Mass fraction Composition	Na/Fe molar ratio			
15	450	0.884(5) $Na_{2.65}Fe_{1.9}(PO_4)_y(SO_4)_{3-y}$	1.39	0.019(6)	0.097(1)	-
	480	0.74(2) $Na_{2.54}Fe_{2.14}(PO_4)_y(SO_4)_{3-y}$	1.19	0.020(1)	0.22(2)	0.020(3)
	510	0.62(1) $Na_{3.55}Fe_{2.7}(PO_4)_y(SO_4)_{3-y}$	1.31	0.120(4)	-	0.26(1)
25	450	0.835(3) $Na_{2.82}Fe_{2.02}(PO_4)_y(SO_4)_{3-y}$	1.40	-	-	0.165(3)

Though the sample obtained at 450°C provides the largest alluaudite's fraction, the possible decomposition of the sulfate part was double-checked. As no solvents were used during the synthesis (dry ball milling, directly followed by thermal treatment) the composition of the sample depends on the chemical composition of the precursor's mixture, which was also verified prior to the synthesis. Indeed, the ICP-OES analysis for the sample obtained by the solid-state method at 450°C during 15 h was conducted and revealed, as expected, a ratio Na : Fe : P : S = 3 : 2: 1: 2 (**Table S1**), with no direct evidence of sulfur loss due to gas evolution. SEM images of this sample (**Figure S1**) show big aggregates of particles with varying sizes. This morphology indicates the need for further ball milling process to reduce particle size in order to ensure optimal electrochemical performance.

Thermal stability tests revealed that $Na_{2.65}Fe_{1.9}(PO_4)_y(SO_4)_{3-y}$ decomposes at 540°C, as shown in the thermogravimetric data in **Figure S2,** even though the mass loss already begins to occur around 460°C. In comparison, the sulfate alluaudite $Na_{2+2\delta}Fe_{2-\delta}(SO_4)_3$ was already formed at temperatures around 300°C [25] and obtained at 350°C [8, 18, 19], and it decomposed at 450°C forming $Na_3Fe(SO_4)_3$ and FeO [26]. Therefore, our results suggest that the presence of the phosphate group enhances the thermal stability of the material. The thermal stability is directly related to the lattice energy and actually to the nature and character of the metal ligand bonds. Sulfate groups being larger and more polarizable than phosphate groups, they are thus more easily decomposed with release of stable gaseous products (SO_3, SO_2, O_2). Partial substitution of sulfate by phosphate

is thus, as observed, a successful route to increase the lattice energy and the thermal stability of mixed polyanion active material.

Synthesis followed in situ by synchrotron X-ray diffraction. To gain further information on the reaction mechanism, *in situ* high-temperature synchrotron X-ray diffraction (SXRD) was carried out. As mentioned in the synthesis protocol, a ball milled mixture of $FeSO_4$ and Na_3PO_4 in molar ratio 2 : 1 was heated in a quartz capillary sealed under argon atmosphere with a heating rate of 3°C/min. In comparison with the described solid-state synthesis procedure, the powder was not pressed for *in situ* experiment and only the heating part without maintaining the temperature fixed was performed. Therefore, differences in alluaudite stoichiometry could be expected. Selected SXRD patterns collected *in situ* during the synthesis of alluaudite, in the temperature range of 50 - 450°C, are presented in **Figure 3**, along with the identified crystalline phases (on the right). The XRD pattern of the precursors' mixture at 50°C reveals that the diffraction peaks of highest intensity correspond to $FeSO_4$ (*S.G. Cmcm*, ICSD #23507) as shown in **Figure S3**, assuming that Na_3PO_4 is amorphous after ball milling mixing, as it is confirmed by an increased background. Other low intensity peaks were not identified, that could be attributed to the formation of intermediate metastable phases, for which mechanochemical synthesis is known for. In the temperature range 50 - 150°C no visible changes were detected, and starting from 150°C, two broad peaks at around 12.3° 2θ and 16.6°2θ appear: their intensity increases with temperature till 400°C. In parallel, $Na_6Fe(SO_4)_4$, frequently reported as a thermodynamically stable impurity in sulfate alluaudite synthesis, is formed at around 250°C.

At 352°C, the sample (**Figure S4**) still contains $Na_6Fe(SO_4)_4$, but no matching peak positions for the previously mentioned intense peaks were found in the databases (PDF4, ICSD, COD). Nevertheless, we observed a resembling match with $Na_{3-\alpha}Fe^{2+}{}_2PO_4(SO_4)_2$, obtained by Na^+ intercalation at C/10 into the thermodynamically stable Fe^{3+}-based NaSICON compound, $NaFe^{3+}{}_2PO_4(SO_4)_2$ (*R*-3 *S.G.* [26,27]), as reported in **Figures S5a,b.** Indeed, as reported in **Figure S6** and **Table S2,** the Le Bail fitting of the SXRD pattern collected *in situ* at 352°C confirms the presence of a NaSICON phase, indexed in the *R*32 *S.G.* with cell parameters a = 9.0681(5) Å, c = 21.887(2) Å, V = 1558.68(6) Å^3, close to cell parameters of $Na_{3-\alpha}Fe_2PO_4(SO_4)_2$, being a = 8.8794(5) Å, c = 21.881(1) Å, V = 1494.0(1) Å^3. The deviation of the cell parameters is likely explained by differences in Na content and P/S ratio between both phases. Therefore, these experiments tend

to demonstrate for the first time the occurrence of a NaSICON-based intermediate phase (called N-NFPS) between 250°C and 400°C, coexisting with $FeSO_4$ and $Na_6Fe(SO_4)_4$.

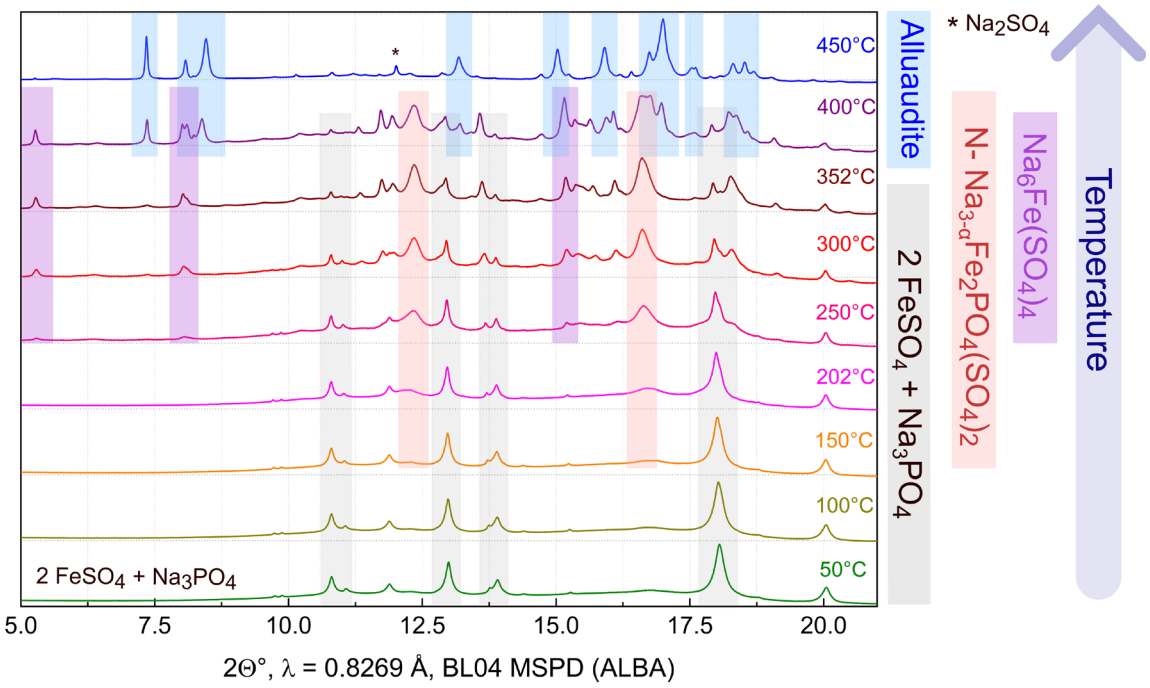

Figure 3. Synthesis followed *in situ* by SXRD in the temperature range 50 - 450°C via heating $FeSO_4$ and Na_3PO_4 in molar ratio 2 : 1. The patterns are presented for every 50°C, identified crystalline phases are highlighted on the right in colorful rectangles: grey corresponds to the initial mixture of $FeSO_4$ and Na_3PO_4, pink to NaSICON-structured $Na_{3-\alpha}Fe_2PO_4(SO_4)_2$, violet to $Na_6Fe(SO_4)_4$ (COD #7130195), and blue to the targeted mixed polyanion alluaudite phase, which final composition is refined as $Na_{2.55}Fe_{2.02}(PO_4)_y(SO_4)_{3-y}$.

In the temperature range 400 - 440°C, all three phases $Na_6Fe(SO_4)_4$, N-NFPS and the newly formed alluaudite are identified, as presented in **Figure S7**. With a slight temperature increase to 450°C, N-NFPS is not detected anymore in significant amounts, while the peaks attributed to $Na_6Fe(SO_4)_4$ are barely detectable. Therefore, 450°C seems to be the optimal temperature for the synthesis of purest alluaudite phase, which composition was refined as $Na_{2.55}Fe_{2.02}(PO_4)_y(SO_4)_{3-y}$. Furthermore, no residues of $FeSO_4$ precursor remain in the sample, as confirmed by the Rietveld refinement of the pattern of the sample obtained at 450°C (**Figure S8**). It is worth noting that the alluaudite NFPS content is 90.3(4) wt%, with minor amounts of impurities of Na_2SO_4 (4.1(1) wt%), $Na_6Fe(SO_4)_4$ (3.7(4) wt%) and Fe_3O_4 (1.9(1) wt%). Lu *et al.* obtained a mixed phase by annealing $Na_2Fe_3(PO_4)_3$ and $Na_2Fe_2(SO_4)_3$ at 350°C for 20 h. In our case, with precursors $FeSO_4$ and Na_3PO_4, a higher temperature of 450°C is required to achieve the purest phase.

The *in situ* temperature-controlled experiment gave direct evidence for the presence of a mixed sodium-rich iron phosphate-sulfate NaSICON-type phase as an intermediate product along with $Na_6Fe(SO_4)_4$ during the synthesis of the alluaudite compound from $FeSO_4$ and Na_3PO_4 under heat treatment. The alluaudite's structure is composed of dimers Fe_2O_{10}, bridged by PO_4/SO_4 tetrahedra, as shown in **Figure 4a**. In the NaSICON structure, the FeO_6 octahedra are not connected directly to each other. Instead, they form lantern units, composed of two FeO_6 octahedra, connected by three PO_4/SO_4 tetrahedra, as presented in **Figure 4b**. Such phase rearrangement could be explained by the higher thermodynamic stability of the alluaudite phase compared to the NaSICON's one, while preserving the same elemental composition. Similar structural transformation from ordered $LiFeSO_4F$ tavorite-type to disordered $LiFeSO_4F$ triplite-type was already observed upon prolonged heating [28]. However, to the best of our knowledge, nothing similar has been previously reported between NaSICON and alluaudite phases. Among synthesized sulfate sodium-rich iron compounds, there are two different crystal structures with very close chemical composition: exceptionally well performing alluaudite $Na_2Fe_2(SO_4)_3$ and NaSICON $Na_{1.84}Fe_2(SO_4)_3$ with poor electrochemical performance [5]. The latter compound was obtained by electrochemical Na^+ intercalation within rhombohedral $Fe^{3+}{}_2(SO_4)_3$, though its structure has not been reported so far.

We believe that this unique observation of intermediate NaSICON phase presence an during synthesis of alluaudite compound can provide valuable insights into influence of synthesis conditions on the stability of a particular structural type. This understanding could also pave the way for the discovery of new positive electrode materials.

Structure and electrochemical properties of the alluaudite phase obtained by solid-state synthesis at 450°C for 15 h.

Crystal structures of obtained compounds. Due to the stabilization of different compositions by numerous explored synthesis methods and conditions, coupled with even various nature of impurities, specific strategies for crystal structure refinements were adopted in each case.

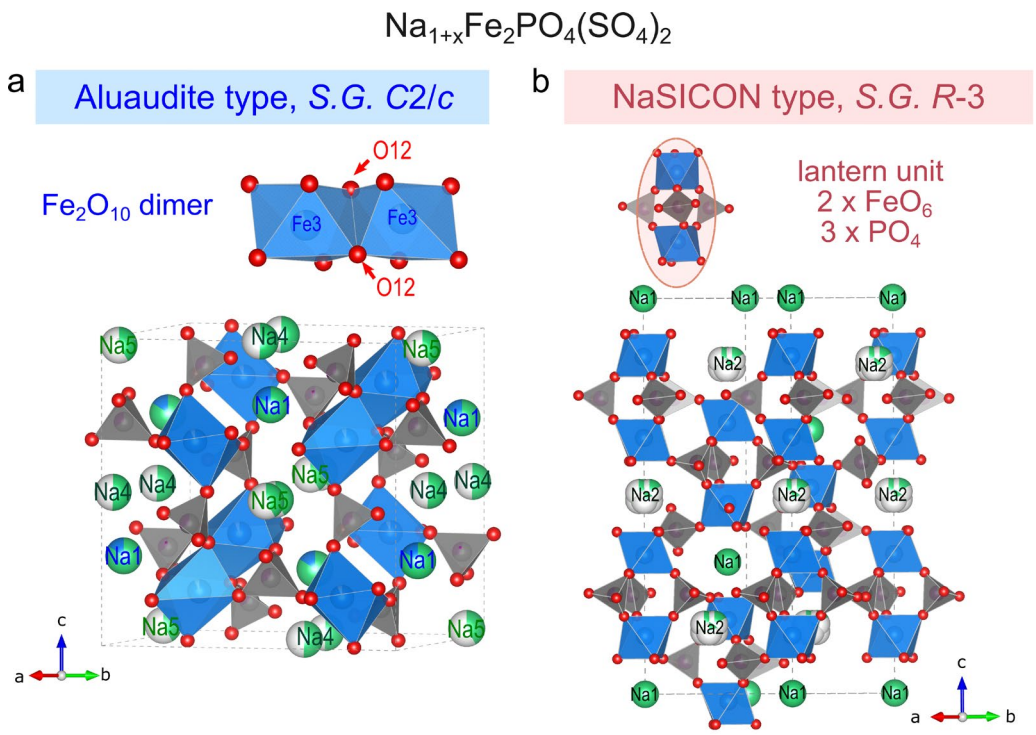

Figure 4. Comparison of crystal structures of mixed phosphate-sulfate of sodium iron in two structural types **(a)** alluaudite with a focus on Fe_2O_{10} dimer, the structural representation of $Na_{2.65}Fe_{1.9}(PO_4)_y(SO_4)_{3-y}$ obtained by solid-state synthesis at 450°C during 15 h; **(b)** NaSICON's structural motif, based on $NaFe_2PO_4(SO_4)_2$, with a building lantern unit [27].

The representation of the crystal structure of the "purest" sample, $Na_{2.65}Fe_{1.9}(PO_4)_y(SO_4)_{3-y}$, obtained by solid-state synthesis at 450°C for 15 h, is given in **Figure 4a**. All the diffraction peaks in its XRD pattern (after "subtraction" of peaks belonging to known impurities) can be indexed in *C*2/*c* (*Z* = 4) space group, as shown in **Figure S9**. Due to its higher sodium content, the cell volume (V = 939.01(1) Å^3) is higher than that of 931.86 Å^3 reported for $Na_{2.37}Fe_{2.15}PO_4(SO_4)_2$ by Lu *et al.*[21], but smaller than that of 951.462 Å^3 found for $Na_{2.9}Fe_{1.7}(SO_4)_{1.7}(PO_4)_{0.3}$ by Liu *et al*. [20] For the Rietveld refinement, the structural model from Lu *et al.* [21] was used as starting model, which suggests the presence of two distinct partially occupied sodium sites (Na4 and Na5), along with one shared site for sodium and iron (Na1/Fe2) and iron site (Fe3) in the dimer with occasional vacancies. At the first step of refinements the atomic displacement parameters (ADP) parameters for the atoms on the Na4 and Na5 4*e* sites were refined independently and always resulted in U_{iso} values of 0.06 Å^2 (B_{iso} ≈ 5 Å^2) or higher, which we considered as too large. As these big values of ADPs for Na atoms could be a sign of lower occupancy or partial disorder of Na atoms, the positions were split from special to general ones (8*f*) that resulted in noticeable shift of sodium atoms, as reported in **Table S3**. Refined ADPs became close to 0.015 Å^2, therefore fixed as 0.02 Å^2 (B_{iso} ≈1.6 Å^2) for the final refinement. The refined value of ADP for the Na1/Fe2 site was close to 0.02 Å^2, which allowed to fix it and to refine its occupancy, yielding a Na1 : Fe2 ratio of 0.82(2)

: 0.18(2). The bond valence sum (BVS) for Na at this position was calculated to be 1.28, slightly higher than expected for Na, corroborating the presence of Fe at this site. For the Fe3 site, located in the dimer, the ADP was refined to be 0.0087 $Å^2$ and fixed to refine its occupancy, yielding 0.86(1). The latter may suggest a presence of vacancies in this site, as suggested in Lu's model[21], with reported variations of occupancy of the Fe3 position in the range from 0.86 to 0.953 depending on S/P ratio. The BVS for Fe at this position was calculated to be 2.2(1), in good agreement with awaited value. Fe3 is coordinated by 6 oxygen atoms, two of them (O12) belonging to the shared edge of Fe_2O_{10} dimer, as highlighted in **Figure 4a** and **Table S3**. Strong Fe3-Fe3 electrostatic repulsion likely accounts for the elongated Fe3-O12 distances of 2.21(2) and 2.266(8) Å, though the mean awaited distance of Fe^{2+}–O bond (CN = 6) is equal [29] to 2.147 Å. Phosphorus and sulfur cannot be distinguished by XRD technique, their occupancies were constrained to the 1 : 2 ratio. The P/S-O bond distances were restrained not to exceed 1.54 ± 0.05 Å. For S6/P7 sites, located at special positions in the initial model, we also discovered elevated refined U_{iso} as 0.045 $Å^2$, which motivated us also to split this position.

In conclusion, the final refinement of Na/Fe ratios provided the composition of alluaudite phase $Na_{2.65}Fe_{1.9}(PO_4)_y(SO_4)_{3-y}$. **Figures S10-14** and **Tables S5-S13** give the structural description obtained for all the alluaudite phases identified in the other samples, the same strategy to that just described (see the SI for more details) was applied in order to specifically determine their contents in Na and Fe, and the phase fraction of the main phase as reported previously in **Table 2**. It is worth noting that all impurities present in the samples, such as Fe_3O_4, $Na_6Fe(SO_4)_4$, Na_2SO_4, are known to accompany pure sulfate sodium iron alluaudites [8, 14, 18, 25], except for those nonidentified in the sample obtained by mechanochemical synthesis. Indeed, its XRD pattern contains at least two additional diffraction peaks non-indexed in *C*2/*c* (at 8.82° and 10.65°2θ, **Figure S11**), that could be attributed to an unidentified impurity. Previously Barpanda *et al*. [8] have shown that the $Na_2Fe_2(SO_4)_3$ structure could be described in both *C*2/*c* and $P2_1/c$ space groups and we thus attempted to refine this XRD pattern in the $P2_1/c$ *S.G.*, which resulted in nonrealistic bond distances. It seems that the mechanochemical synthesis ensures the biggest degree of mixing of Na/Fe with domination of Fe in this position and thus providing a Na/Fe ratio of 0.93. From the structural point of view, longer annealing at 450°C (25 h vs. 15 h) does not change the Na/Fe ratio, though in absolute values it varies. Furthermore, disorder on the P/S site and on the Na4 and Na5 sites, as observed in the sample obtained during 15 h annealing, is not observed anymore in the sample obtained during 25 h, as could be observed from comparison of **Tables S3** and **S12**.

Fe local environment and oxidation state. To further characterize the $Na_{2.65}Fe_{1.9}(PO_4)_y(SO_4)_{3-y}$ phase and to determine the local environment and oxidation state of Fe atoms in the mixed polyanion alluaudite, a Mössbauer spectrum of the sample was collected (**Figure 5**).

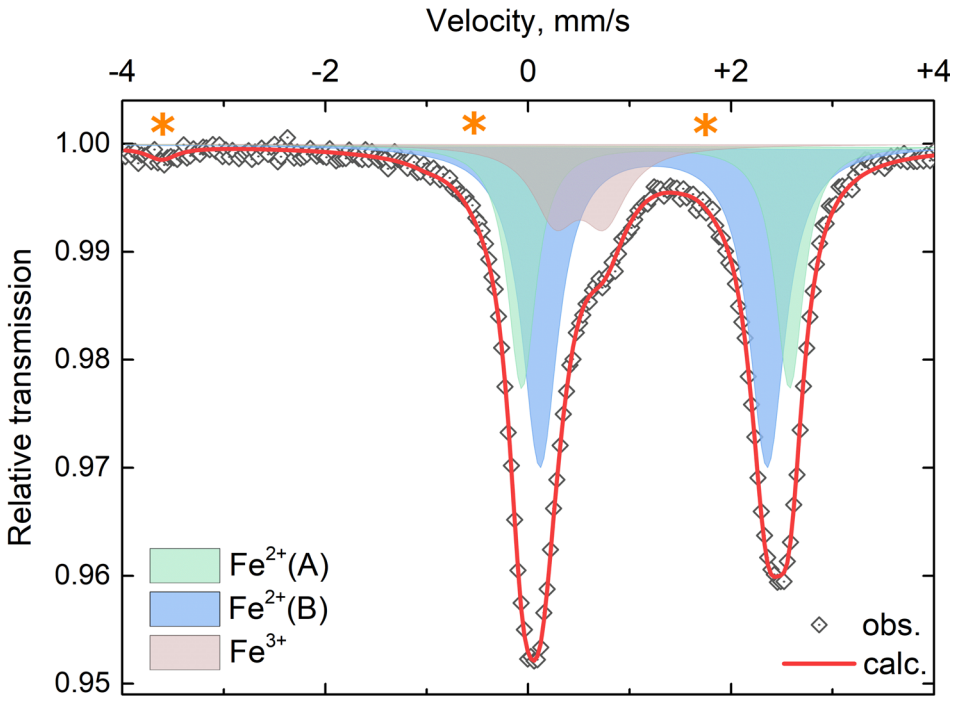

Figure 5. Room temperature ^{57}Fe Mössbauer spectrum collected for $Na_{2.65}Fe_{1.9}(PO_4)_y(SO_4)_{3-y}$. The corresponding refined hyperfine parameters are reported in Table 3. The contribution of Fe_3O_4 sextets is marked by orange asterisks, as presented in **Figure S15**.

Table 3. Hyperfine parameters of ^{57}Fe Mössbauer spectrum of $Na_{2.65}Fe_{1.9}(PO_4)_y(SO_4)_{3-y}$ (T = 298K), where δ is the isomer shift, Δ the quadrupolar splitting and Γ the line width. The hyperfine parameters of Fe_3O_4 were fixed [30].

Component	δ, mm/s	Δ, mm/s	Γ, mm/s	Area, %
Fe^{3+}	0.51(3)	0.49(3)	0.53(3)	14(3)
Fe^{2+} (A)	1.26(1)	2.64(2)	0.32(2)	29(3)
Fe^{2+} (B)	1.24(1)	2.24(2)	0.43(2)	50(3)
Fe_3O_4 (1)	0.27(-)	0.05(-)	0.37(-)	2(3)
Fe_3O_4 (2)	0.67(-)	-0.02(-)	0.37(-)	5(3)

The experimental spectrum was reconstructed with three main components: one minor Fe^{3+} component and two Fe^{2+} components, named as Fe^{2+}(A) and Fe^{2+} (B), with corresponding hyperfine parameters reported in **Table 3**. Besides, a minor amount of Fe_3O_4 (≈ 3%), also detected by XRD, was identified on the spectrum. The fraction of Fe^{3+} in the alluaudite phase was estimated

as 14% by Mössbauer spectroscopy, thus yielding an alluaudite composition of $Na_{2.65}Fe_{1.9}(PO_4)_{0.72}(SO_4)_{2.28}$ with formation of a sulfate-rich phase. It should be noted, though, that the amount of Fe^{3+} in the phase at room temperature is usually overestimated due to the difference of Lamb-Mössbauer factors [31]. The isomer shift (δ) values for Fe^{3+} and the two Fe^{2+} components are characteristic of six-fold coordinated high-spin Fe^{3+} ($t^3_{2g}e^2_g$) and Fe^{2+} ($t^4_{2g}e^2_g$) in an oxygen environment [30].

Table 4. Comparison of ^{57}Fe Mössbauer hyperfine parameters (T = 298K) of sulfate and phosphate sodium iron alluaudites from literature data. δ is the isomer shift, Δ the quadrupolar splitting and Γ the line width. * Quadrupole splitting distribution was adopted.

Compound	Type	Fraction	δ, mm/s	Δ, mm/s	Γ, mm/s	Reference
$Na_2Fe_2(SO_4)_3$	Fe^{2+} (1)	0.5	1.2798(8)	2.378(3)	0.396(3)	8
	Fe^{2+} (2)	0.5	1.2798(8)	1.954(3)	0.382(4)	
$Na_{2.56}Fe_{1.72}(SO_4)_3$	Fe^{2+} (1)	0.96	1.2797(6)	2.20*	0.25	18
$Na_{2.5}Fe_{1.75}(SO_4)_3$	Fe^{2+} (1)	1.00	1.280(1)	2.20(1)	-	32
$NaFe_{3.67}(PO_4)_3$	Fe^{2+}	0.57	1.22	2.08	0.42	33
	Fe^{2+}	0.29	1.24	2.40	0.36	
	Fe^{3+}	0.14	0.50	0.38	0.34	
$Na_2Fe_3(PO_4)_3$	Fe^{2+}	0.64	1.94(3)	3.86(6)	-	34
	Fe^{3+}	0.36	0.41(4)	1.35(8)	-	
$Na_{2.65}Fe_{1.9}(PO_4)_y(SO_4)_{3-y}$	Fe^{2+} (A)	0.31(3)	1.26(1)	2.64(2)	0.32(2)	this work
	Fe^{2+} (B)	0.54(3)	1.24(1)	2.24(2)	0.43(2)	
	Fe^{3+}	0.15(3)	0.51(3)	0.49(3)	0.53(3)	

As reported in **Table 4**, the δ values for the Fe^{2+} components are slightly lower than those observed for off-stochiometric sodium iron sulfate alluaudites, but higher than those reported for Fe^{2+} in phosphate alluaudites, supporting the formation of a mixed phosphate-sulfate phase. As XRD data on average Fe–O bond lengths do not provide clear evidence regarding the distribution of Fe^{3+} and Fe^{2+} atoms between the shared Na1/Fe2 and Fe3 positions, it is therefore difficult to assign specific oxidation states of iron to distinct crystallographic sites. The spherical distribution of electronic charge of high-spin Fe^{3+} results in a quadrupole splitting (Δ) influenced by the distortion of FeO_6 octahedra and surrounding cationic environment. As the Δ value of Fe^{3+} of 0.49(3) mm/s is not extremely high in comparison, for example, with 1.35(8) mm/s in the spectrum of $Na_2Fe_3(PO_4)_3$, one may speculate that Fe^{3+} atoms could be located in the position

Fe3 with more regular oxygen environment than Na1/Fe2. Conversely, the large Δ values observed for the Fe^{2+} components indicate significant distortion in their octahedral environments, possibly linked to disorder involving Na and Fe atoms, as well as P/S as representatives of second coordination sphere.

Electrochemical properties.

To investigate electrochemical properties of the mixed phosphate-sulfate alluaudites, samples were tested as positive electrodes in Na-half cells at 25°C. The theoretical capacity of $Na_{2.65}Fe_{1.9}(PO_4)_y(SO_4)_{3-y}$ is approximately estimated to 111 mAh/g (assuming all Fe atoms undergo redox processes), and corresponds to the exchange of 1.9 mol of e^- per formula unit. Therefore, the expected capacity of our material ($Na_{2.65}Fe_{1.9}(PO_4)_y(SO_4)_{3-y}$) is higher than the theoretical capacity of $Na_{2.9}Fe_{1.7}(SO_4)_{1.7}(PO_4)_{0.3}$ alluaudite (101.3 mAh/g) reported by Liu *et al*.[20]

Figure 6a presents charge and discharge profiles obtained in the 2.2 - 4.5 V vs. Na^+/Na voltage range at varying discharge rates (from C/30 to 2C), with all the charges performed at C/30, where 1C = 111 mA g^{-1}. The data show smooth voltage profiles, suggesting solid solution mechanism upon Na^+ (de-)intercalation, typical for alluaudite sulfate and phosphate-based compounds [8,20,21] . The electrode material exhibits a reversible capacity of 93 mAh/g at C/30 for the 1st cycle, which is equal to 82% of the theoretical capacity. One can note that the first charge capacity of 89.7 mAh/g at C/30 is slightly lower than the discharge capacity (93 mAh/g), which supports the presence of a low amount of Fe^{3+} electrochemically active species in the pristine NFPS. Importantly, the reversible capacity gradually increases over the first 15 cycles of the rate capability test, suggesting a slow activation process and an enhancement of the electrolyte impregnation during initial cycling. This phenomenon is likely attributed to the high electrode mass loading (≈20 mg/cm^2) we used for lab-scale experiments, and suggests that further optimization in the electrode preparation could be conducted. Despite the high mass loading, the electrode still delivers a reversible capacity of 95 mAh/g at C/5 and 61 mAh/g at 1C, revealing a promising rate capability. Then, following the rate capability test, electrochemical cycling at C/30 restored 87% of the initial capacity, as shown in **Figure 6b**. The average voltage is estimated at 3.32 V vs. Na^+/Na, which is rather close to the 3.43 V reported by Lu *et al.* for the composition $Na_{2.37}Fe_{2.15}PO_4(SO_4)_2$ [21]. Finally, prolonged electrochemical cycling stability of the sample was also evaluated using two different protocols as illustrated in **Figure 6c:** first, both cells were cycled for 5 cycles at C/30; subsequently, one cell was cycled for 15 cycles at C/10 and the other for 45

cycles at C/5. In both cases, a similar slight increase in discharge capacity during cycling was noted, as observed in the rate capability test. Crucially, no capacity loss was observed during this extended cycling, underscoring the exceptional stability of this polyanion material under prolonged operation. In conclusion, these preliminary electrochemical tests demonstrate that $Na_{2.65}Fe_{1.9}(PO_4)_y(SO_4)_{3-y}$ holds significant promise as a positive electrode material for Na-ion batteries. Its composition, based on abundant and non-toxic elements, along with encouraging electrochemical performance and stability, makes it an attractive candidate. Nevertheless, further optimization of the electrode preparation process is expected to enhance its performance for in-depth evaluation of its performance in full cell set-up and larger format cells.

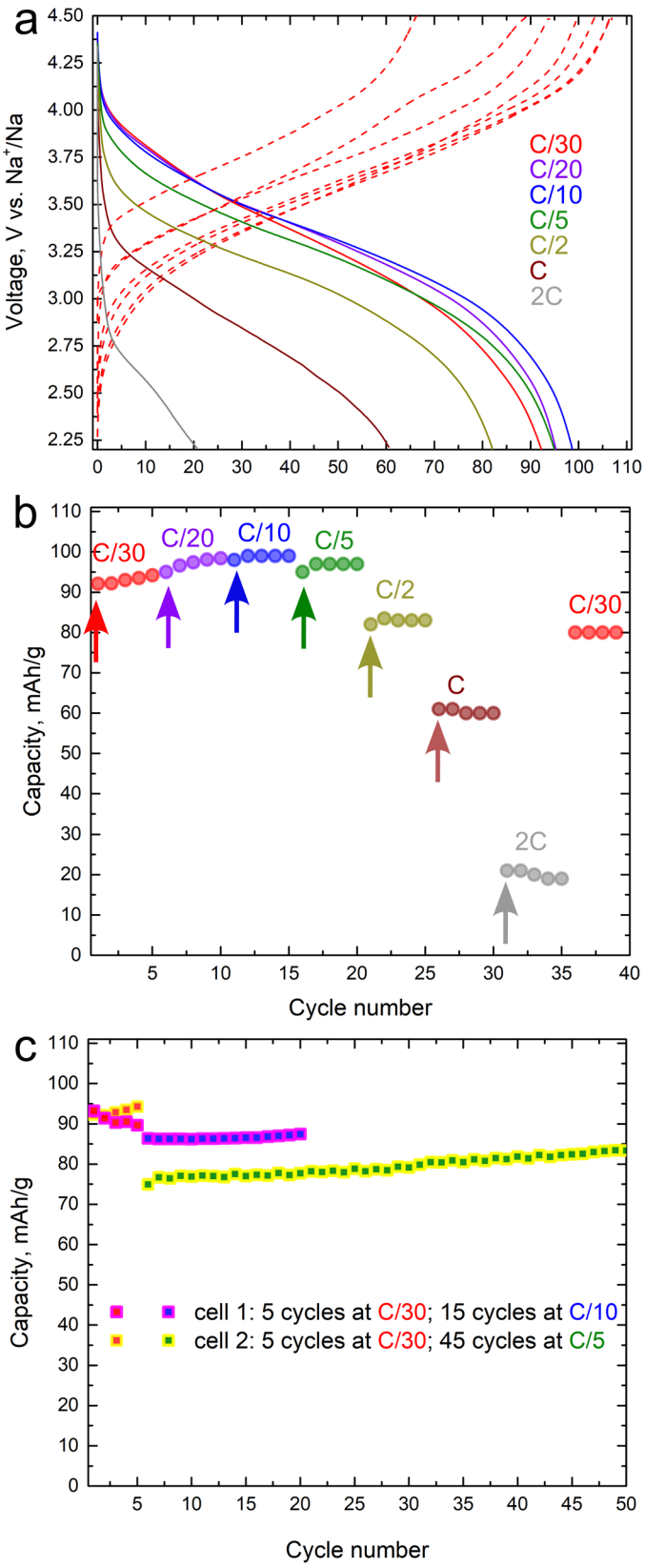

Figure 6: (a) Galvanostatic charge/discharge curves of NFPS//Na half-cells: the charges plotted in dash lines were performed at a rate of C/30, followed by discharges in continuous lines performed at rates of C/30 to 2C. **(b)** Capacity retention observed at different discharge rates. Arrows highlight particular discharge profiles, plotted in (a). **(c)** Capacity evolution of NFPS in Na half-cells

following two different cycling protocols: firstly, 5 cycles at C/30; subsequently the 1st cell was charged and discharged for 15 cycles at C/10 (pink squares) and the 2nd cell was charged and discharged for 45 cycles at C/5 (yellow squares).

Conclusion

With a view to address the growing demand for cost-effective and efficient energy storage devices, we proposed new compositions within the mixed phosphate-sulfate iron sodium alluaudite system as positive electrode materials for Na-ion batteries. We demonstrated the feasibility of synthesis of these alluaudite phases using two inexpensive and sustainable precursors, Na_3PO_4 and $FeSO_4$, via three methods, such as mechanochemical, ionothermal and solid-state. To gain insights into the reaction mechanisms, the phase formation process was monitored by temperature *in situ* Synchrotron X-ray diffraction. The results revealed that the mixed phosphate-sulfate alluaudite phase is formed already at 400°C and is obtained almost pure at 450°C. This work reports, for the first time, the observation of an intermediate NaSICON phase prior to alluaudite formation. Optimization of solid-state synthesis conditions, *i.e.* 450°C for 15 h, provided the purest sample (88 wt%), with a chemical formula $Na_{2.65}Fe_{1.9}(PO_4)_y(SO_4)_{3-y}$, as confirmed by XRD and Mössbauer spectroscopy.

The combination of phosphate and sulfate groups enhances the thermal stability of the phase compared to sulfate compounds, while maintaining high average discharge voltage of 3.32 V vs. Na^+/Na, attributed to the inductive effect of sulfate groups. When tested as a positive electrode material in Na-half cell, the material delivered 92 mAh/g (active mass loading of 20 mg/cm^2), which corresponds to 83% of the theoretical capacity (110.6 mAh/g). Additionally, it exhibited very promising long-term stability and rate capability.

In summary, we present novel synthesis procedures, unveiled mechanism of solid-state synthesis reaction, and conducted structural investigations of new mixed phosphate-sulfate iron sodium alluaudites, based on abundant elements, positioning them as promising materials for Na-ion batteries.

Supporting information: ICP-OES results, SEM & TGA data on $Na_{2.65}Fe_{1.9}(PO_4)_y(SO_4)_{3-y}$; additional XRD pattern, collected *in situ* during synthesis; crystallographic details on refinements.

Acknowledgements

Emmanuel Petit, Jérôme Kalisky, Cathy Denage, Matthew Suchomel, Eric Lebraud and Stan Pechev from ICMCB are recognized for their technical and scientific support for the experimental lab management, X-ray diffraction, scanning electron microscopy, and chemical and thermal analyses. As part of the DESTINY PhD Program, A.G., J.O., L.S., C.M. and L.C, acknowledge the funding from the European Union's Horizon2020 research and innovation program under the Marie Skłodowska-Curie Actions COFUND (Grant Agreement #945357). A.G. also acknowledges the funding and financial support from the CEA LITEN, as well as A.G., J.O., C.M. and L.C. that of the French National Research Agency (STORE- EX Labex Project ANR- 10-LABX-76-01). The Région Nouvelle Aquitaine is thanked for the cofounding of most of the characterization equipment used in this study, and the authors also acknowledge Alba-Cells Synchrotron facility for providing beamtime at the MSPD beamline (Proposals No. 2023097893 and 2024028348) for powder X-ray diffraction and Alexander Missyul for help during these beamtimes. A.G. would like to thank Roman Shpanchenko for XRD discussions.

References

(1) Larcher, D.; Tarascon, J. M. Towards Greener and More Sustainable Batteries for Electrical Energy Storage. *Nat. Chemistry.* **2015**, 19–29. https://doi.org/10.1038/nchem.2085.

(2) Vaalma, C.; Buchholz, D.; Weil, M.; Passerini, S. A Cost and Resource Analysis of Sodium-Ion Batteries. *Nat. Rev. Mater.* **2018**, 3, 18013 (11 pages). https://doi.org/10.1038/natrevmats.2018.13.

(3) Yabuuchi, N.; Kajiyama, M.; Iwatate, J.; Nishikawa, H.; Hitomi, S.; Okuyama, R.; Usui, R.; Yamada, Y.; Komaba, S. P2-Type $Na_x[Fe_{1/2}Mn_{1/2}]O_2$ Made from Earth-Abundant Elements for Rechargeable Na Batteries. *Nat. Mater.* **2012**, 11 (6), 512–517. https://doi.org/10.1038/nmat3309.

(4) Xu, C.; Zhou, L.; Gao, T.; Chen, Z.; Hou, X.; Zhang, J.; Bai, Y.; Yang, L.; Liu, H.; Yang, C.; Zhao, J.; Hu, Y. S. Development of High-Performance Iron-Based Phosphate Cathodes toward Practical Na-Ion Batteries. *J. Am. Chem. Soc.* **2024**, 146 (14), 9819–9827. https://doi.org/10.1021/jacs.3c14452.

(5) Chung, S. C.; Ming, J.; Lander, L.; Lu, J.; Yamada, A. Rhombohedral NASICON-Type $Na_xFe_2(SO_4)_3$ for Sodium Ion Batteries: Comparison with Phosphate and Alluaudite Phases. *J. Mater. Chem. A.* **2018**, 6 (9), 3919–3925. https://doi.org/10.1039/c7ta08606g.

(6) Slater, P. R.; Greaves, C. Powder Neutron Diffraction Study of the Nasicon-Related Phases $Na_xM^{II}_xM^{III}_{2-x}(SO_4)_{3-y}(SeO_4)_y$: M^{II}=Mg, M^{III}= Fe, In. *J. Mater. Chem.* **1994**, 4 (9), 1469–1473. https://doi.org/10.1039/JM9940401469.

(7) Masquelier, C.; Wurm, C.; Rodríguez-Carvajal, J.; Gaubicher, J.; Nazar, L. A Powder Neutron Diffraction Investigation of the Two Rhombohedral NASICON Analogues: γ-$Na_3Fe_2(PO_4)_3$ and $Li_3Fe_2(PO_4)_3$. *Chem. Mater.* **2000**, 12 (2), 525–532. https://doi.org/10.1021/cm991138n.

(8) Barpanda, P.; Oyama, G.; Nishimura, S. I.; Chung, S. C.; Yamada, A. A 3.8-V Earth-Abundant Sodium Battery Electrode. *Nat. Commun.* **2014**, 5, 4358 (8 pages). https://doi.org/10.1038/ncomms5358.

(9) Trad, K.; Carlier, D.; Croguennec, L.; Wattiaux, A.; Ben Amara, M.; Delmas, C. $NaMnFe_2(PO_4)_3$ Alluaudite Phase: Synthesis, Structure, and Electrochemical Properties As Positive Electrode in Lithium and Sodium Batteries. *Chem. Mater.* **2010**, 22 (19), 5554–5562. https://doi.org/10.1021/cm1015614.

(10) Meng, Y.; Yu, T.; Zhang, S.; Deng, C. Top-down Synthesis of Muscle-Inspired Alluaudite $Na_{2+2x}Fe_{2-x}(SO_4)_3$/SWNT Spindle as a High-Rate and High-Potential Cathode for Sodium-Ion Batteries. *J. Mater. Chem. A.* **2016**, 4 (5), 1624–1631. https://doi.org/10.1039/c5ta07696j.

(11) Barman, P.; Dwibedi, D.; Jayanthi, K.; Meena, S. S.; Nagendran, S.; Navrotsky, A.; Barpanda, P. Aqueous Spray-Drying Synthesis of Alluaudite $Na_{2+2x}Fe_{2-x}(SO_4)_3$ Sodium Insertion Material: Studies of Electrochemical Activity, Thermodynamic Stability, and Humidity-Induced Phase Transition. *J. Solid State Electrochem.* **2022**, 26 (9), 1941–1950. https://doi.org/10.1007/s10008-022-05142-w.

(12) Plewa, A.; Kulka, A.; Hanc, E.; Zając, W.; Sun, J.; Lu, L.; Molenda, J. Facile Aqueous Synthesis of High Performance $Na_2FeM(SO_4)_3$ (M = Fe, Mn, Ni) Alluaudites for Low Cost Na-Ion Batteries. *J. Mater. Chem. A.* **2020**, 8 (5), 2728–2740. https://doi.org/10.1039/c9ta11565j.

(13) Jungers, T.; Mahmoud, A.; Malherbe, C.; Boschini, F.; Vertruyen, B. Sodium Iron Sulfate Alluaudite Solid Solution for Na-Ion Batteries: Moving towards Stoichiometric $Na_2Fe_2(SO_4)_3$. *J. Mater. Chem. A.* **2019**, 7 (14), 8226–8233. https://doi.org/10.1039/c9ta00116f.

(14) Yang, W.; Liu, Q.; Yang, Q.; Zhang, X.; Yang, Z.; Mu, D.; Li, L.; Chen, R.; Wu, F. Uncovering the Nonequilibrium Evolution Mechanism between $Na_{2+2\delta}Fe_{2-\delta}(SO_4)_3$ Cathode and Impurities in the Na_2SO_4-$FeSO_4{\cdot}7H_2O$ Binary System for High-Voltage Sodium-Ion Batteries. *Small.* **2024**, 20, 2405982. https://doi.org/10.1002/smll.202405982.

(15) Dwibedi, D.; Ling, C. D.; Araujo, R. B.; Chakraborty, S.; Duraisamy, S.; Munichandraiah, N.; Ahuja, R.; Barpanda, P. Ionothermal Synthesis of High-Voltage Alluaudite $Na_{2+2x}Fe_{2-x}(SO_4)_3$ Sodium Insertion Compound: Structural, Electronic, and Magnetic Insights. *ACS Appl. Mater. Interfaces.* **2016**, 8 (11), 6982–6991. https://doi.org/10.1021/acsami.5b11302.

(16) Abakumov, A. M.; Fedotov, S. S.; Antipov, E. V.; Tarascon, J. M. Solid State Chemistry for Developing Better Metal-Ion Batteries. *Nat. Commun.* **2020**, 11 (4976). https://doi.org/10.1038/s41467-020-18736-7.

(17) Gutierrez, A.; Benedek, N. A.; Manthiram, A. Crystal-Chemical Guide for Understanding Redox Energy Variations of $M^{2+}/^{3+}$ Couples in Polyanion Cathodes for Lithium-Ion Batteries. *Chem. Mater.* **2013**, 25 (20), 4010–4016. https://doi.org/10.1021/cm401949n.

(18) Oyama, G.; Nishimura, S.; Suzuki, Y.; Okubo, M.; Yamada, A. Off-Stoichiometry in Alluaudite-Type Sodium Iron Sulfate $Na_{2+2x}Fe_{2-x}(SO_4)_3$ as an Advanced Sodium Battery Cathode Material. *ChemElectroChem*. **2015**, 2 (7), 1019–1023. https://doi.org/10.1002/celc.201500036.

(19) Zhang, J.; Yan, Y.; Wang, X.; Cui, Y.; Zhang, Z.; Wang, S.; Xie, Z.; Yan, P.; Chen, W. Bridging Multiscale Interfaces for Developing Ionically Conductive High-Voltage Iron Sulfate-Containing Sodium-Based Battery Positive Electrodes. *Nat. Commun.* **2023**, 14 (3701). https://doi.org/10.1038/s41467-023-39384-7.

(20) Liu, C.; Chen, K.; Li, F.; Zhao, A.; Chen, Z.; Fang, Y.; Cao, Y. Anion-Doped $Na_{2.9}Fe_{1.7}(SO_4)_{2.7}(PO_4)_{0.3}$ Cathode with Improved Cyclability and Air Stability for Low-Cost Sodium-Ion Batteries. *Nano Energy*. **2024**, 125 (109557). https://doi.org/10.1016/j.nanoen.2024.109557.

(21) Lu, J.; Nishimura, S.; Yamada, A. Polyanionic Solid-Solution Cathodes for Rechargeable Batteries. *Chem. Mater.* **2017**, 29 (8), 3597–3602. https://doi.org/10.1021/acs.chemmater.7b00226.

(22) Liu, C.; Chen, K.; Li, F.; Zhao, A.; Liu P.; Chen, Z.; Fang, Y.; Cao, Y. Unlocking Phase Purity of Sodium Iron Sulfate for Low-Cost and High-Performance Sodium-Ion Batteries. *J. Am. Chem. Soc.* **2025**, 147 (17), 14635–14646. https://doi.org/10.1021/jacs.5c02485.

(23) Toby, B. H.; Von Dreele, R. B. GSAS-II: The Genesis of a Modern Open-Source All Purpose Crystallography Software Package. *J. Appl. Crystallogr.* **2013**, 46 (2), 544–549. https://doi.org/10.1107/S0021889813003531.

(24) Fauth, F.; Peral, I.; Popescu, C.; Knapp, M. The New Material Science Powder Diffraction Beamline at ALBA Synchrotron. *Powder Diffr.* **2013**, 28 (S2), 360–370. https://doi.org/10.1017/S0885715613000900.

(25) Plewa, A.; Kulka, A.; Baster, D.; Molenda, J. An Alluaudite Compounds $Na_2Fe_2(SO_4)_3$ vs. $Na_{2.5}Fe_{1.75}(SO_4)_3$ as Earth Abundant Cathode Materials for Na-Ion Batteries. *Solid State Ionics.* **2019**, 335, 15–22. https://doi.org/10.1016/j.ssi.2019.02.007.

(26) Ben Yahia, H.; Essehli, R.; Amin, R.; Boulahya, K.; Okumura, T.; Belharouak, I. Sodium Intercalation in the Phosphosulfate Cathode $NaFe_2(PO_4)(SO_4)_2$. *J. Power Sources*. **2018**, 382, 144–151. https://doi.org/10.1016/j.jpowsour.2018.02.021.

(27) Grebenshchikova A.; Olchowka J.; Simonin L.; Duttine M.; Weill F.; Suard E.; Masquelier C.; Croguennec L. NaSICON $NaFe_2PO_4(SO_4)_2$ Revisited: Insights into the Crystal Structure and Electrochemical Performance. *ACS Appl. Energy Mater.* 2025, 8 (18), 13620–13630, https://doi.org/10.1021/acsaem.5c01935.

(28) Ati, M.; Sathiya, M.; Boulineau, S.; Reynaud, M.; Abakumov, A.; Rousse, G.; Melot, B.; Van Tendeloo, G.; Tarascon, J. M. Understanding and Promoting the Rapid Preparation of the Triplite-Phase

of $LiFeSO_4F$ for Use as a Large-Potential Fe Cathode. *J. Am. Chem. Soc.* **2012**, 134 (44), 18380–18387. https://doi.org/10.1021/ja3074402.

(29) Gagné, O. C.; Hawthorne, F. C. Bond-Length Distributions for Ions Bonded to Oxygen: Results for the Transition Metals and Quantification of the Factors Underlying Bond-Length Variation in Inorganic Solids. *IUCrJ.* **2020**, 7, 581–629. https://doi.org/10.1107/S2052252520005928.

(30) Menil, F. Systematic Trends of the 57Fe Mössbauer Isomer Shifts in (FeO_n) and (FeF_n) Polyhedra. Evidence of a New Correlation between the Isomer Shift and the Inductive Effect of the Competing Bond T-X (-Fe) (Where X Is O or F and T Any Element with a Formal Positive Charge). *J. Phys. Chem. Solids.* **1985**, 46 (7), 763–789. https://doi.org/10.1016/0022-3697(85)90001-0.

(31) De Grave, E.; Alboom, A. Van. Evaluation of Ferrous and Ferric Mössbauer Fractions. *Phys. Chem. Minerals.* **1991**, 18, 337–342. https://doi.org/10.1007/BF00200191.

(32) Wei, S.; Mortemard de Boisse, B.; Oyama, G.; Nishimura, S. I.; Yamada, A. Synthesis and Electrochemistry of $Na_{2.5}(Fe_{1-y}Mn_y)_{1.75}(SO_4)_3$ Solid Solutions for Na-Ion Batteries. *ChemElectroChem.* **2016**, 3 (2), 209–213. https://doi.org/10.1002/celc.201500455.

(33) Korzenski, M. B.; Schimek, G. L.; Kolis, J. W.; Long, G. J. Hydrothermal Synthesis, Structure, and Characterization of a Mixed-Valent Iron(II/III) Phosphate, $NaFe_{3.6}(PO_4)_3$: A New Variation of the Alluaudite Structure Type. *J. Solid State Chem.* **1998**, 139, 152–160. https://doi.org/10.1006/jssc.1998.7823.

(34) Huang, W.; Li, B.; Saleem, M. F.; Wu, X.; Li, J.; Lin, J.; Xia, D.; Chu, W.; Wu, Z. Self-Assembled Alluaudite $Na_2Fe_{3-x}Mn_x(PO_4)_3$ Micro/Nanocompounds for Sodium-Ion Battery Electrodes: A New Insight into Their Electronic and Geometric Structure. *Chem. Europ. J.* **2015**, 21 (2), 851–860. https://doi.org/10.1002/chem.201403062.